Energy & Environmental Science

Accepted Manuscript

ROYAL SOCIETY OF CHEMISTRY

www.rsc.org/ees

Journal Name RSCPublishing

COMMUNICATION

Cite this: DOI: 10.1039/x0xx00000x

Received 00th January 2012,
Accepted 00th January 2012

DOI: 10.1039/x0xx00000x

www.rsc.org/

High Efficiency Flexible Perovskite Solar Cells using Superior Low Temperature TiO_2

Dong Yang,[a] Ruixia Yang,[b] Jing Zhang,[b] Zhou Yang,[a] Shengzhong (Frank) Liu*[a,b] and Can Li*[b]

A process is developed to prepare very dense TiO_2 layer using magnetron sputtering at room temperature. It is found that the film is amorphous in nature, offering faster electron transport, reduced transfer resistance and better performance in electron extraction from the perovskite absorber layer. It is these superior electronic properties that makes it possible for us to achieve 15.07% efficiency flexible perovskite solar cells, on respectably large area >10 mm^2. It is the highest efficiency reported to date for the flexible perovskite devices.

The perovskite solar cells, due to its low cost, high efficiency and straightforward architecture, are promising candidates to revolutionize future photovoltaic markets.[1-5] In only a few years after its invention, the power conversion efficiency (PCE) of the perovskite cells has rapidly increased to ~20.1%,[6-12] thanks to the strong light absorption, weakly bound excitons, long range charge-carrier diffusion and apparent tolerance to defects.[13-17] The electron transport layer (ETL), also serves as the hole blocking layer, is a key component in high efficiency planar perovskite solar cells. It needs to be highly transparent across the solar spectrum (at least in most of visible region) and to offer good electron extraction ability, low carrier transfer resistance and an energy level matching the conduction band of the perovskite material. A few ETLs have been developed for high efficiency perovskite cells, most notably TiO_2, ZnO, mesoscopic ZrO_2 and Al_2O_3.[18-20] Even though high initial cell efficiency has been made using the ZnO ETL without high temperature sintering, but its stability is very poor.[21] With the mesoscopic ZrO_2 and Al_2O_3 ETLs, the resultant solar cells exhibits good stability in ambient air under full sunlight, unfortunately, these materials required high-temperature sintering, and their insulating properties result in large resistance for the electrons generated in absorber layer to transfer to the ETL and then to the cathode, consequently reduced short-circuit current density (J_{sc}).[22,23]

Anatase-TiO_2 (an-TiO_2) has been successfully used, unfortunately, there are two major challenges: (i) The TiO_2 films are usually deposited using spray pyrolysis or spin coating techniques,[24,25] requiring a high-temperature sintering (> 450 ℃) to achieve relatively dense structure and meanwhile the amorphous oxide layer transforms into the crystalline anatase.[26-28] Obviously, this high temperature process is not compatible with common polymeric substrates and complicates the fabrication. A few advanced deposition techniques have therefore been developed, e.g. atomic layer deposition, sol-gel, microwave sintering, high-pressure pressing and electro-deposition,[29-33] regrettably, the performance is still lower than that using traditional high-temperature TiO_2. (ii) Even though there are indeed reports on high PCE perovskite cells using an-TiO_2 ETLs,[11,34] the Fermi level of the an-TiO_2, about -4.0 eV, is likely so close to the conduction band of the perovskite material that the difference is too small to facilitate effective electron injection from the absorber layer and therefore limiting the solar cell performance.[35] It is critical to explore the possibility of fabricating ETLs with suitable Fermi level at low temperature.

In this work, we report our development of a dense amorphous TiO_2 (am-TiO_2) film at room temperature. The am-TiO_2 film is highly transparent across the solar spectrum. It is found to offer improved electron injection and reduced transfer resistance at the cathode interface. Besides, the Fermi level of the am-TiO_2 film matches well with the conduction band of the perovskite material. Using the am-TiO_2 film, we have fabricated flexible planar perovskite solar cells with efficiency as high as 15.07%, on respectably large area >10 mm^2, significantly higher than the best record reported to date (~12.2%).[36,37] Moreover, the rigid perovskite solar cells were fabricated using the am-TiO_2 ETL based on glass/ fluorine-doped tin oxide (FTO) substrates, with maximum efficiency of 16.22% and average PCE is 15.64%, higher than that using the an-TiO_2 (15.35%) ETL prepared with same process condition.

The device structure for this study is illustrated in Fig. 1a. The transparent electrode, either FTO or indium tin oxid (ITO) is used as the bottom cathode, and the 2,2′,7,7′-tetrakis(N,N-di-p-methoxyphenylamine)-9,9′-spirobifluorene (spiro-OMeTAD)/Au bilayer as the top anode. The homogeneous $CH_3NH_3PbI_{3-x}Cl_x$ layer was deposited as absorber layer with full coverage on different substrates (Fig. S1). The process details are given in the supporting information. In brief, the $PbCl_2$ film (Fig S2) was deposited using a thermal evaporation system. It was then placed onto a layer of CH_3NH_3I powder. Upon a heat treatment at 150 ℃ for 20 min, the perovskite is formed. Five diffraction peaks in X-ray diffraction (XRD) patterns, centred at 14.15 °, 28.48 °, 31.92 °, 43.24 ° and 60.90 °, are assigned to (110), (220), (310), (330) and (440) diffractions,[38] respectively (Fig. S3). The TiO_2 film is employed as ETL in the perovskite solar cell.

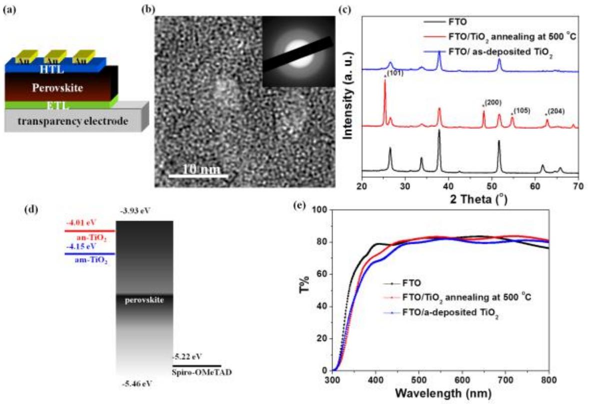

Fig. 1. (a) The device structure of the planar perovskite solar cell. (b) HRTEM image and electron diffraction pattern (inset) of the as-deposited TiO_2 film. (c) GI-WAXS spectra of the as-deposited TiO_2 films and the FTO/TiO_2 annealed at 500 ℃ for 30 min. (d) Energy level diagram of the components of the perovskite solar cell with an-TiO_2 or am-TiO_2 as ETL. (e) Optical transmission spectra of the FTO, FTO/an-TiO_2 and FTO/am-TiO_2 films.

Fig. 1b shows the high resolution transmission electron microscopy (HRTEM) image and electron diffraction pattern of the as-deposited TiO_2 film. There is no sign of crystalline grains in the image. Meanwhile, the electron diffraction pattern of the as-deposited TiO_2 film shows only diffused background with no distinctive bright spots that can be assigned to crystal planes. In addition, Fig. 1c displays the grazing-incidence wide-angle X-ray scattering (GI-WAXS) data of the as-deposited TiO_2 on FTO and the film after annealing at 500 ℃ for 30 min. For the best sensitivity, the 10 keV X-ray beam was incident at a grazing angle of 1 ° from the sample. It appears that the as-deposited TiO_2 film on the FTO gives no additional peaks beyond what already existed from the substrate, indicating that the as-deposited TiO_2 film is amorphous. However, after being annealed at 500 ℃ for 30 min, additional peaks show up at 25.37 °, 48.12 °, 53.97 ° and 62.74 °, corresponding to the (101), (200), (105) and (204) diffractions from an-TiO_2 phase.[39,40] It is clear, based on the HRTEM, electron diffraction and GI-WAXS, that the as-deposited TiO_2 film is indeed amorphous.

The Fermi levels of the TiO_2 films in different forms were measured by Kelvin Probe Force Microscopy (KPFM). Fig. 1d displays the energy level diagram of materials in the perovskite solar cells. The Fermi level of the am-TiO_2 film is -4.15 eV, slightly deeper than -4.01 eV for the an-TiO_2 film (Fig. S4). The neutral oxygen vacancies can be formed during preparation of the am-TiO_2 films by DC magnetron sputtering. Such oxygen vacancies produce occupied impurity density of states above the valence band.[41] The conduction band and valence band drop and the Fermi level is shifted down to the valence band,[41,42] leading to the deeper Fermi level (-4.15 eV) in am-TiO_2. The oxygen vacancies are filled by oxygen in the ambient after thermal annealing,[41,42] yielding a Fermi level of -4.01 eV in an-TiO_2. Consequently, the electrons can be more easily injected into the am-TiO_2 film from the absorber layer due to the relative large disruption in energy levels between the conduction band of perovskite material and the Fermi level of ETL. The scanning electron microscopy (SEM) and atom force microscopy (AFM) images of the an-TiO_2 and am-TiO_2 films are shown in Fig. S5. The morphology of an-TiO_2 films is similar to that of am-TiO_2 films on the FTO substrate. The surface root-mean-square (RMS) roughness decreases from 13.93 nm to ca. 12.7 nm when the FTO was covered by the TiO_2 film. The smoother surface is believed to be beneficial to electric contact between the perovskite film and the ETL. Fig. 1e reveals the optical transmission spectra of the FTO, FTO/an-TiO_2 and FTO/am-TiO_2 films. Both an-TiO_2 and am-TiO_2 films on the FTO show high transmittance > 78% in average in the wavelength range 400-800 nm, allowing maximum photo flux to reach the absorber layer for photon-generated carriers.

The excellent performance inspired us to fabricate flexible perovskite solar cells using the am-TiO_2 ETLs on flexible poly(ethylene terephthalate) (PET)/ITO substrates. Fig. 2a illustrates a photograph of a flexible perovskite solar cell using the am-TiO_2 ETL on flexible PET/ITO substrate. Fig. 2b shows the current-density voltage (J-V) curves of the perovskite solar cells using both flexible PET/ITO and rigid glass/ITO substrates. The key J-V parameters of the devices are summarized in Table 1. The rigid device exhibits the J_{sc} of 21.68 mA cm^{-2}, open-circuit voltage (V_{oc}) of 1.03 V and fill factor (FF) of 0.72, giving the PCE of 16.08%. The PCE of the flexible perovskite solar cell is 15.07% with a J_{sc} = 20.90 mA cm^{-2}, V_{oc} = 1.03 V and FF = 0.70. It is worthwhile to note that the PCE on large area >10 mm^2 is higher than the best efficiency reported up to date for the flexible perovskite cells.[36,37,43-46] A careful study shows that the slightly lower PCE comparing to that of the rigid device is due to the decreased J_{sc} and FF, likely caused by the higher series resistance and lower transmittance of the PET/ITO substrate in short wavelength spectrum (Fig. S6). Fig. 2c confirms that the photon-to-electron conversion efficiency (IPCE) of the flexible device is indeed slightly smaller than that of the rigid cell. The performance of the flexible device does not degrade even after mechanical bending towards about 65 ° for 100 times, as shown in Fig. 2b, indicating that the flexible devices show good mechanical stability. To further confirm the reproducibility of the flexible perovskite solar cells, 15 individual devices were fabricated and their J-V characteristics analyzed. The PCE distribution histogram is shown in Fig. 2d, demonstrating very good reproducibility with limited variation (see Table S1 for detailed statistics).

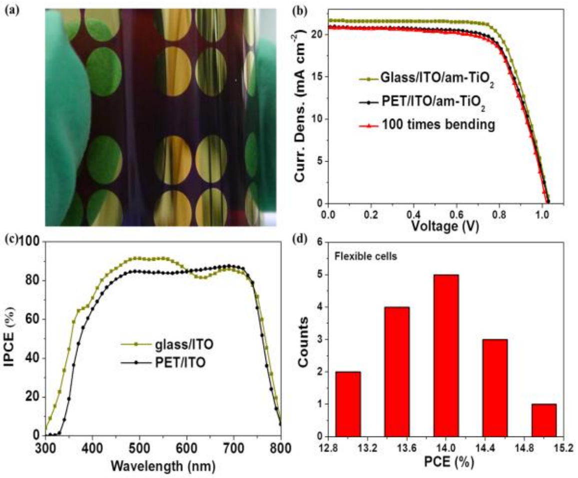

Fig. 2. (a) A photograph of a flexible perovskite solar cell. (b) J-V curves of the rigid and flexible devices with am-TiO_2 as ETLs and the flexible device before and after 100 bending cycles. (c) IPCE curves of the rigid and flexible perovskite solar cells. (d) The PCE distribution histogram of the flexible perovskite solar cells.

Table 1. The parameters of the perovskite solar cells without and with different ETLs.

Substrate/ETL	J_{sc} (mA cm^{-2})	V_{oc} (V)	FF	PCE (%)
Glass/ITO/am-TiO_2	21.68	1.03	0.72	16.08
PET/ITO/am-TiO_2	20.90	1.03	0.70	15.07
Glass/FTO w/o	16.29	0.89	0.50	7.25
Glass/FTO/an-TiO_2	20.90 ±0.80	1.08 ±0.01	0.68 ±0.01	15.35 ±0.43
Champion device	21.67	1.08	0.69	16.10
Glass/FTO/am-TiO_2	21.60 ±0.32	1.02 ±0.01	0.71 ±0.01	15.64 ±0.25
Champion device	21.87	1.03	0.72	16.22

To study the impact of the an-TiO_2 and am-TiO_2 on device performance, the planar perovskite solar cells were fabricated using glass/FTO substrates. Note that the ITO was not chosen for it would suffer great performance drop at the high temperature to form crystalline anatase. Fig. 3a displays the J-V curves of the devices under AM 1.5G illumination at 100 mW cm^{-2}. Photovoltaic parameters including J_{sc}, V_{oc}, FF and PCE are summarized in Table 1. The control device without the ETL gives a J_{sc} = 16.29 mA cm^{-2}, V_{oc} = 0.89 V, and FF = 0.50, resulting in a PCE = 7.25%. The inferior performance of perovskite solar cells without the ETL is attributed to serious recombination caused by the direct contact between the absorber layer and the cathode. It is found that the J_{sc} increased with the deeper Fermi level of the ETL, from 20.90 mA cm^{-2} for an-TiO_2 to 21.60 mA cm^{-2} for the am-TiO_2. Fig. 3b shows the comparison of the IPCE of the perovskite solar cells with and without ETLs. It is believed that the relatively high IPCE and J_{sc} are due to the better property including high transmittance, suitable energy level and smooth surface of the am-TiO_2 ETL which allows more efficient electron transfer from the perovskite materials. Comparing to the am-TiO_2 ETL, the FF is decreased from 0.71 to 0.68 with the an-TiO_2 ETL. The V_{oc} is decreased to 1.02 V when using the am-TiO_2, comparing to 1.08 V for the an-TiO_2. According to previous reports, the V_{oc} is determined by the difference between the Fermi level of ETL and hole transport layer (HTL).[35,47-49] As the difference for the am-TiO_2 is smaller than that of the an-TiO_2, as shown in Fig. 1b, the smaller V_{oc} for the am-TiO_2 ETL is expected. However, the average PCE of the devices based on am-TiO_2 ETLs increased to 15.64% from 15.35% for the an-TiO_2 with the improved J_{sc} and FF, regardless of the reduced V_{oc}. To further confirm the reproducibility of the perovskite solar cells based on different ETLs, 15 individual devices were fabricated and analyzed. The PCE distribution histograms are shown in Fig. S7, validate that the PCE is highly reproducible with little variation (listed in Table S1). The best PCE is as high as 16.22% (J_{sc}=21.87 mA cm^{-2}, V_{oc}=1.03 V FF=0.72), as shown in Fig. 3c and Table 1. Note that the perovskite solar cell based on the an-TiO_2 shows a lower champion PCE of 16.10% (Fig. 3d and Table 1). Meanwhile, Fig. 3c and 3d displays the effect of scanning condition, including both reverse and forward scan directions, on the J-V characteristics of the champion perovskite solar cell using different ETLs. Note that the scan rate used was 0.2 V s^{-1}. It is believed that the hysteresis may be originated from the defects within the perovskite layer.[50,51] To obtain a more reliable PCE, Fig. 3e and 3f shows the photocurrent density and PCE of the champion devices using an-TiO_2 and am-TiO_2 ETLs measured as a function of time at a forward bias set at their respective V_{mp} (voltage at the maximum power point in the J-V curve, in this case 0.78 V for an-TiO_2 and 0.76 V for am-TiO_2). The PCE of the champion device using am-TiO_2 is 15.73%, while that of the an-TiO_2 is 15.53%, over 100 s measurement window. These values are very close to the PCE obtained from the reverse scan for the J-V measurement.

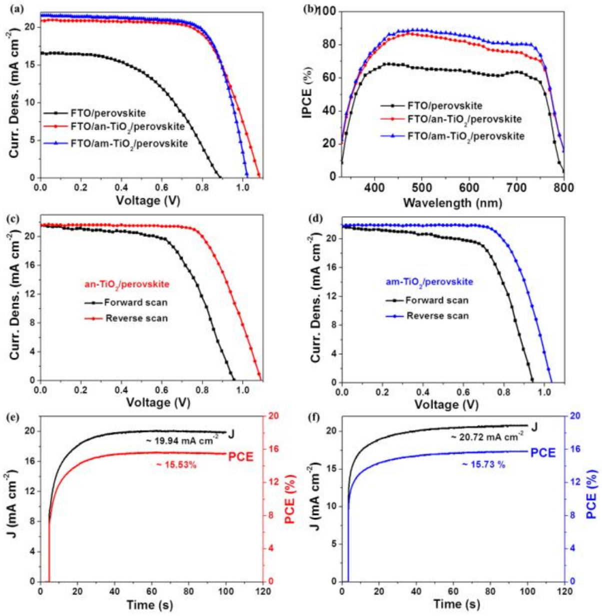

Fig. 3. (a) J-V characteristics of the perovskite solar cells without or with various ETLs under AM 1.5G irradiation at 100 mW cm^{-2}. (b) IPCE curves of the perovskite solar cells without or with various ETLs. J-V curves including reverse and forward scan directions of the champion devices based on (c) an-TiO_2 ETL and (d) am-TiO_2 ETLs. Photocurrent density and PCE measured as a function of time for the same cells biased at 0.78 V for (e) an-TiO_2 and 0.76 V for (f) am-TiO_2. The cells were kept in the dark under open-circuit prior to the measurement.

The steady state photoluminescence (PL) measurements can reveal the photo-induced charge transfer and charge recombination loss. Fig. 4a shows the PL spectra of the glass/perovskite, an-TiO_2/perovskite and am-TiO_2/perovskite films. The glass/perovskite film has the highest PL intensity, indicating the serious recombination in the perovskite film. The PL intensity of am-TiO_2/perovskite film is weaker comparing to that of an-TiO_2/perovskite film, indicating that the charge transfer effectively occurred before the carrier recombination at interface and that the am-TiO_2 ETL improves electron extraction from the absorber layer. To gain more insight into the fundamental reason why the am-TiO_2 ETL is better than the an-TiO_2 for the perovskite solar cells, time-resolved photoluminescence (TRPL) spectroscopy was measured using the time-correlated single photon counting (TCSPC) method at a fixed acquisition time. Fig. 4b displays the TRPL spectra of different substrates in perovskite layers. The PL decay time and amplitudes are obtained using an exponential Eq. (1)

$$f(t) = \sum_i A_i \exp(-t/\tau_i) + K \qquad (1)$$

where A_i is the decay amplitude, τ_i is the decay time and K is a constant for the base-line offset.

To understand the recombination mechanism of the perovskite thin films on different substrates, the recombination kinetics was modelled over a range of excitation intensities using the following Eq. (2)

$$-\frac{dn}{dt} = An + Bn^2 + Cn^3 \qquad (2)$$

where n is the photogenerated excess carrier density and t is the time.[52,53] The physical interpretations of these three terms are (i) the first-order decay rate is due to the trap-mediated (Shockley−Hall-Read) recombination at low injection condition; (ii) the second-order decay rate is due to the non-geminate/free carrier recombination at high injection; and (iii) the third order decay rate is for the Auger recombination. The glass/perovskite data are collected without injection, hence the strong second-order decay rate from Eq. (2) is negligible. When TiO_2/perovskite is analyzed, the tremendous second-order decay rate is observed for the photogenerated carrier easy injection from perovskite to the TiO_2 ETL. Based on the above analysis, the PL decay time of glass/perovskite obtained by single-exponential model, and bi-exponential function is used to fit the PL decay time of perovskite coated on TiO_2. Parameters of the TRPL data based on glass/perovskite, an-TiO_2/perovskite and am-TiO_2/perovskite are listed in Table S2. For the glass/perovskite sample, the PL decay time is 20.98 ns, consistent with previous reports.[4,] The long decay time is essential for long exciton diffusion length and low density of defects in the perovskite thin film.[45,54] The PL decay time of an-TiO_2/perovskite are τ_1=17.34 ns and τ_2= 4.71 ns, the corresponding amplitudes are 25.27% and 74.73%, respectively. For the am-TiO_2/perovskite, the τ_1 and τ_2 drop to 12.68 ns and 1.66 ns. Compared to the an-TiO_2/perovskite sample, the amplitude of the relatively long decay time is sharply reduced to 4.68%, while the corresponding amplitude to the fast decay time increased to 95.32%. The average recombination lifetime (τ_{ave}) are estimated with the τ_i and A_i values from the fitted curve data (Table S2) using the Eq. (3).[55]

$$\tau_{ave} = \frac{\sum Ai\tau_i^2}{\sum Ai\tau_i} \qquad (3)$$

Comparing to the glass/perovskite sample, the PL decay time is significantly reduced when the perovskite film is coated on TiO_2 ETLs. The average decay time using the an-TiO_2 ETL decreased to 11.72 ns. It further drops to 4.68 ns when the am-TiO_2 ETL is used, demonstrating that the electrons transfer faster from the perovskite film to am-TiO_2 ETL, comparing to the an-TiO_2 ETL, as witnessed by stronger steady state PL quenching in the am-TiO_2/perovskite sample (Fig. 4a). It is apparent that the electrons can efficient transfer from the perovskite absorber layer into am-TiO_2 due to relative larger disruption in energy levels between the conduction band of perovskite materials and the Fermi level of the am-TiO_2 ETL.

Assuming that both radiative and non-radiative decay processes of perovskite are associated with TiO_2 ETL, the observed fast lifetime can be correlated to the rate for interfacial electron transfer by Eq. (4)

$$k_{et} = \frac{1}{\tau_{ads}} - \frac{1}{\tau_{un}} \qquad (4)$$

where k_{et} is the specific rate constant for the charge injection process, τ_{ads} is emission lifetime for the TiO_2/perovskite, τ_{un} is emission lifetime for the pristine perovskite film. It turned out that the electron injection rate from perovskite to am-TiO_2 is 1.66×10^8 s^{-1}, an order of magnitude faster than that for the an-TiO_2 (3.77×10^7 s^{-1}) (Table S2), demonstrating that the efficient electron transfer from the perovskite to am-TiO_2 ETL.

As the faster electron injection rate from perovskite to the am-TiO_2 ETL is beneficial to the charge separation at the perovskite/ETL interface, it is expected that charge recombination would be effectively suppressed, leading to higher J_{sc} and FF in device performance.

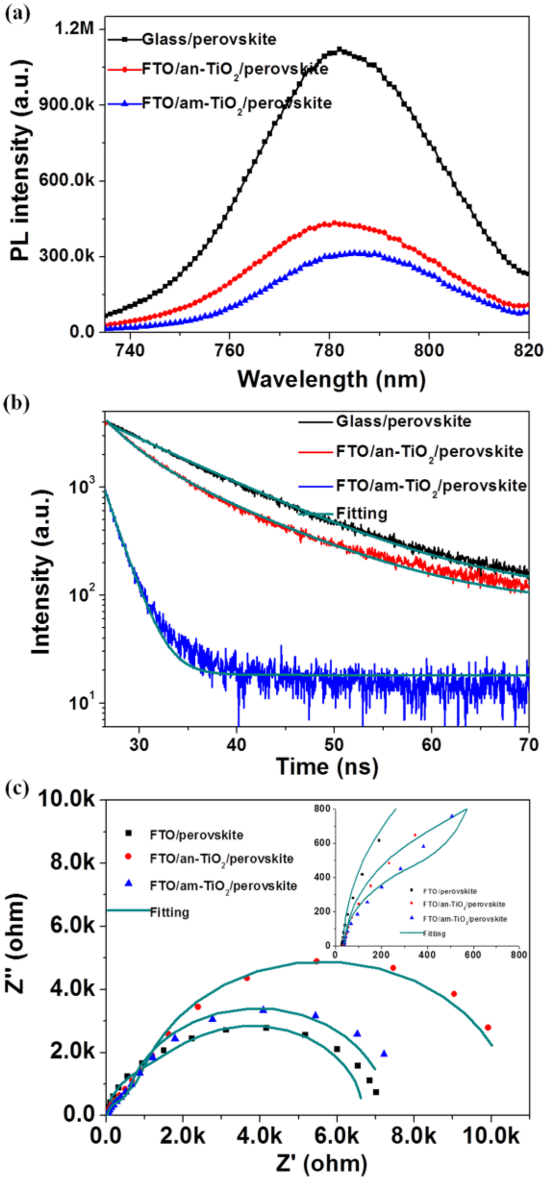

Fig. 4. (a) Steady state PL spectra of the glass/perovskite, FTO/an-TiO_2/perovskite and FTO/am-TiO_2/perovskite films. (b) PL decay profiles of different substrates in perovskite layers. (c) Nyquist plot of perovskite solar cells with and without ETLs with the upper-right inset showing the EIS zoomed in to the high-frequency region.

Furthermore, electrical impedance spectroscopy (EIS) is used to study the interface charge tranport in the perovskite solar cells.[56] The ETLs can forcefully reduce the transfer resistance between the FTO and the perovskite films, as shown in Fig. 4c. The Nyquist plots of the devices were measured at 0.80 V in dark and the equivalent circuit model for the perovskite solar cells is shown in Fig. S8. The fitted equivalent circuit model is composed of series resistance (R_s), two components for transfer resistance (R_{tr}) at the ETL/perovskite and the perovskite/HTL interfaces, and recombination resistance (R_{rec}) forming a parallel circuit with capacitors (C_{tr} and C_{rec}). The R_{tr} is ascribed to high-frequency arc and the R_{rec} assigned to low-frequency arc. Given that the perovskite/HTL interface is identical in all cases, the R_{tr} is mainly associated with the TiO_2/perovskite interface, hence its value reflects the electron extraction/transport properties at the perovskite/ETL interfaces. The parameters of the equivalent circuit with different ETLs are summarized in Table S3. It is clear that the device without ETL exhibits the largest R_{tr} of 1337 Ω and the smallest R_{rec} of 5303 Ω, indicating poor electron transport properties and serious carrier recombination processes, as witnessed by the lowest J_{sc} and V_{oc}. The R_{tr} is found to be notably decreased to 504.1 Ω for the perovskite solar cells based on the am-TiO_2 comparing to 779.1 Ω of that using the an-TiO_2 ETL (the upper-right inset of Fig. 4c), implying more efficient extraction/transport of the electrons at the am-TiO_2/perovskite interface. Comparing to the an-TiO_2 ETL, the am-TiO_2 ETL significantly improves electron injection and reduces transfer resistance, resulting in increased J_{sc} and FF for the solar cells.

Conclusions

We have demonstrated an effective am-TiO_2 ETL prepared at room temperature for the perovskite solar cells. The PCE for the flexible perovskite solar cell is raised to as high as 15.07% using the am-TiO_2 ETL. The good performance of the perovskite solar cells based on am-TiO_2 ETLs is attributed to improved electron injection and reduced transfer resistance. Fabrication of the am-TiO_2 film at room temperature makes it possible to develop interfaces of perovskite solar cells and offers potential application in other photoelectronic device.

Acknowledgements

The authors acknowledge support from the National University Research Fund (GK261001009), the Changjiang Scholar and Innovative Research Team (IRT_14R33), the Overseas Talent Recruitment Project (B14041) and the Chinese National 1000-talent-plan program.

Notes and references

[a] Key Laboratory of Applied Surface and Colloid Chemistry, National Ministry of Education; Institute for Advanced Energy Materials, School of Materials Science and Engineering, Shaanxi Normal University, Xi’an 710119, China

[b] State Key Laboratory of Catalysis, Dalian National Laboratory for Clean Energy, Dalian Institute of Chemical Physics, Chinese Academy of Sciences, Dalian, 116023, China

*E-mail: szliu@dicp.ac.cn; canli@dicp.ac.cn

Electronic Supplementary Information (ESI) available: [details of any supplementary information available should be included here]. See DOI:10.1039/c000000x/

1 M. M. Lee, J. Teuscher, T. Miyasaka, T. N. Murakami and H. J. Snaith, *Science*, 2012, **338**, 643.

2 J. H. Im, C. R. Lee, J. W. Lee, S. W. Park and N. G. Park, *Nanoscale*, 2011, **3**, 4088.

3 W. Nie, H. Tsai, R. Asadpour, J. C. Blancon, A. J. Neukirch, G. Gupta, J. J. Crochet, M. Chhowalla, S. Tretiak, M. A. Alam, H. L. Wang and A. D. Mohite, *Science*, 2015, **347**, 522.

4 D. Zhong, B. Cai, X. Wang, Z. Yang, Y. Xing, S. Miao, W. H. Zhang and C. Li, *Nano Energy*, 2015, **11**, 409.

5 B. J. Pellet, S. J. Moon, R. Humphry-Baker, P. Gao, M. K. Nazeeruddin and M. Grätzel, *Nature*, 2013, **499**, 316.

6 A. Kojima, K. Teshima, Y. Shirai and T. Miyasaka, *J. Am. Chem. Soc.*, 2009, **131**, 6050.

7 N. J. Jeon, J. H. Noh, Y. C. Kim, W. S. Yang, S. Ryu and S. Seok, *Nat. Mater.*, 2014, **13**, 897.

8 J. H. Im, I. H. Jang, N. Pellet, M. Grätzel and N. P. Park, *Nat. Nanotechnology*, 2014, **9**, 927.

9 N. J. Jeon, J. H. Noh, W. S. Yang, Y. C. Kim, S. Ryu, J. Seo and S. Seok, *Nature*, 2015, **517**, 476.

10 Y. Deng, E. Peng, Y. Shao, Z. Xiao, Q. Dong and J. Huang, *Energy Environ. Sci.*, 2015, **8**, 1544.

11 N. J. Jeon, H. G. Lee, Y. C. Kim, J. Seo, J. H. Noh, J. Lee, S. Seok, *J. Am. Chem. Soc.*, 2014, **136**, 7837.

12 www.nrel.gov/ncpv/images/efficiency_chart.jpg, 2015.

13 F. Hao, C. C. Stoumpos, D. H. Cao, R. P. H. Chang and M. G. Kanatzidis, *Nat. photonics*, 2014, **8**, 489.

14 D. Yang, Z. Yang, W. Qin, Y. Zhang, S. Liu and C. Li, *J. Mater. Chem. A*, 2015, **3**, 9401.

15 G. Xing, N. Mathews, S. Sun, S. S. Lim, Y. M. Lam, M. Grätzel, S. Mhaisalkar and T. C. Sum, *Science*, 2013, **342**, 344.

16 Q. Lin, A. Armin, R. C. R. Nagiri, P. L. Burn and P. Meredith, *Nat. photonics*, 2015, **9**, 106.

17 H. S. Kim, C. R. Lee, J. H. Im, K. B. Lee, T. Moehl, A. Marchioro, S. J. Moon, R. Humphry-Baker, J. H. Yum, J. E. Moser, M. Grätzel and N. G. Park, *Scientific Reports*, 2012, **2**, 591.

18 H. Zhou, Q. Chen, G. Li, S. Luo, T. B. Song H. S. Duan, Z. Hong, J. You, Y. Liu and Y. Yang, *Science*, 2014, **345**, 542.

19 D. Liu and T. L. Kelly, *Nat. photonics*, 2013, **8**, 133.

20 A. Mei, X. Li, L. Liu, Z. Ku, T. Liu, Y. Rong, M. Xu, M. Hu, J. Chen, Y. Yang, M. Grätzel and H. Han, *Science*, 2014, **345**, 295.

21 Q. Hu, J. Wu, C. Jiang, T. Liu, X. Que, R. Zhu and Q. Gong, *ACS Nano*, 2014, **8**, 10161.

22 J. T.-W. Wang, J. M. Ball, E. M. Barea, A. Abate, J. A. Alexander-Webber, J. Huang, M. Saliba, I. Mora-Sero, J. Bisquert, H. J. Snaith and R. J. Nicholas, *Nano Lett.*, 2013, **14**, 724.

23 D. Bi, S. J. Moon, L. Häggman, G. Boschloo, L. Yang, E. M. J. Johansson, M. K. Nazeeruddin, M. Grätzel and A. Hagfeldt, *RSC Advances*, 2013, **3**, 18762.

24 G. E. Eperon, V. M. Burlakov, A. Goriely and H. J. Snaith, *ACS Nano*, 2014, **8**, 591.

25 Q. Chen, H. P. Zhou, Z. R. Hong, S. Luo, H. S. Duan, H. H. Wang, Y. S. Liu, G. Li and Y. Yang, *J. Am. Chem. Soc.*, 2014, **136**, 622.

26 C. Y. Li, T. C. Wen, T. H. Lee, T. F. Guo, J. C. A. Huang, Y. C. Lin and Y. J. Hsu, *J. Mater. Chem.*, 2009, **19**, 1643.

27 S. K. Hau, H. L. Yip, O. Acton, N. S. Baek, H. Ma and A. K. Y. Jen, *J. Mater. Chem.*, 2008, **18**, 5113.

28 H. Sun, J. Weickert, H. C. Hesse and L. Schmidt-Mende, *Sol. Energy Mater. & Sol. Cells*, 2011, **95**, 3450.

29 M. Durr, A. Schmid, M. Obermaier, S. Rosselli, A. Yasuda and G. Nelles, *Nat. Mater.*, 2005, **4**, 607.

30 Y. J. He, G. J. Zhao, B. Peng and Y. F. Li, *Adv. Funct. Mater.*, 2010, **20**, 3383.

31 X. L. Hu, G. S. Li and J. C. Yu, *Langmuir*, 2010, **26**, 3031.

32 J. N. Hart, D. Menzies, Y. B. Cheng, G. P. Simon and L. Spiccia, *J. Sol-Gel Sci. Technol.*, 2006, **40**, 45.

33 K. Wojciechowski, M. Saliba, T. Leijtens, A. Abate and H. J. Snaith, *Energy Environ. Sci.*, 2014, **7**, 1142.

34 F. Huang, Y. Dkhissi, W. Huang, M. Xiao, I. Benesperi, S. Rubanov, Y. Zhu, X. Lin, L. Jiang, Y. Zhou, A. Gray-Weale, J. Etheridge, C. R.

McNeill, R. A. Caruso, U. Bach, L. Spiccia and Y.-B. Cheng, *Nano Energy*, 2014, **10**, 10-18.

35 S. Ryu, J. H. Noh, N. J. Jeon, Y. C. Kim, W. S. Yang, J. Seo and S. Seok, *Energy Environ. Sci*., 2014, **7**, 2614.

36 Y. Chen, T. Chen and L. Dai, *Adv. Mater.*, 2015, **23**, 1053.

37 B. J. Kim, D. H. Kim, Y.-Y. Lee, H.-W. Shin, G. S. Han, J. S. Hong, K. Mahmood, T. K. Ahn, Y.-C. Joo, K. S. Hong, N.-G. Park, S. Lee and H. S. Jung, *Energy Environ. Sci.*, 2015, **8**, 916.

38 B. W. Park, B. Philippe, T. Gustafsson, K. Sveinbjornsson, A. Hagfeldt, E. M. J. Johansson and G. Boschloo, *Chem. Mater.*, 2014, **26**, 4466.

39 C. Y. Li, T. C. Wen, T. H. Lee, T. F. Guo, J. C. A. Huang, Y. C. Lin and Y. J. Hsu, *J. Mater. Chem.*, 2009, **19**, 1643.

40 D. Yang, P. Fu, F. Zhang, N. Wang, J. Zhang and C. Li, *J. Mater. Chem. A*, 2014, **2**, 17281.

41 H. H. Pham and L. W. Wang, *Phys. Chem. Chem. Phys.*, 2015, **17**, 541.

42 B. Prasai, B. Cai, M. K. Underwood, J. P. Lewis and D. A. Drabold, *J. Mater. Sci.*, 2012, **47**, 7515.

43 P. W. Liang, C. Y. Liao, C. C. Chueh, F. Zuo, S. T. Williams, X. K. Xin, J. Lin and A. K. Y. Jen, *Adv. Mater.*, 2014, **26**, 3748.

44 C. Roldan-Carmona, O. Malinkiewicz, A. Soriano, G. M. Espallargas, A. Garcia, P. Reinecke, T. Kroyer, M. I. Dar, M. K. Nazeeruddine, H. J. Bolink, *Energy Environ. Sci.*, 2014, **7**, 994.

45 J. You, Z. Hong, Y. M. Yang, Q. Chen, M. Cai, T. B. Song, C. Chen, S. Lu, Y. Liu, H. Zhou and Y. Yang, *ACS Nano*, 2014, **8**, 1674.

46 S. Ryu, J. Seo, S. S. Shin, Y. C. Kim, N. J. Jeon, J. H. Noh and S. Seok, *J. Mater. Chem. A*, 2015, **3**, 3271.

47 B. Cai, Y. Xing, Z. Yang, W. H. Zhang and J. Qiu, *Energy Environ. Sci.*, 2013, **6**, 1480.

48 V. D. Mihailetchi, P. W. M. Blom, J. C. Hummelen and M. T. Rispens, *J. App. Phys.*, 2003, **94**, 6849.

49 J. H. Heo, S. H. Im, J. H. Noh, T. N. Mandal, C. S. Lim, J. A. Chang, Y. H. Lee, H. Kim, A. Sarkar, M. K. Nazeeruddin, M. Grätzel and S. Seok, *Nat. Photonics*, 2013, **7**, 486.

50 H.-S. Kim, I. Mora-Sero, V. Gonzalez-Pedro, F. Fabregat-Santiago, E. J. Juarez-Perez and N.-G. Park, J. Bisquert, *Nat. Commun.*, 2013, **4**, 2242.

51 H. J. Snaith, A. Abate, J. M. Ball, G. E. Eperon, T. Leijtens, N. K. Noel, S. D. Stranks, J. T.-W. Wang, K. Wojciechowski and W. Zhang, *J. Phys. Chem. Lett.*, 2014, **4**, 1511.

52 J. S. Manser and P. V. Kamat, *Nat. photonics*, 2014, **8**, 737.

53 B. S. Tosun and H. W. Hillhouse, *J. Phys. Chem. Lett.*, 2015, **6**, 2503.

54 S. D. Stranks, G. E. Eperon, G. Grancini, C. Menelaou, M. J. P. Alcocer, T. Leijtens, L. M. Herz, A. Petrozza and H. J. Snaith, *Science*, 2013, **342**, 341.

55 S. Gonzalez-Carrero, R. E. Galian and J. Perez-Prieto, *J. Mater. Chem. A*, 2015, **3**, 9187.

56 D. Liu, J. Yang and T. L. Kelly, *J. Am. Chem. Soc.*, 2014, **136**, 17116.

Table of content

High Efficiency Flexible Perovskite Solar Cells using Superior Low Temperature TiO_2

15.07% efficiency for flexible perovskite solar cell achieved using low temperature TiO_2.

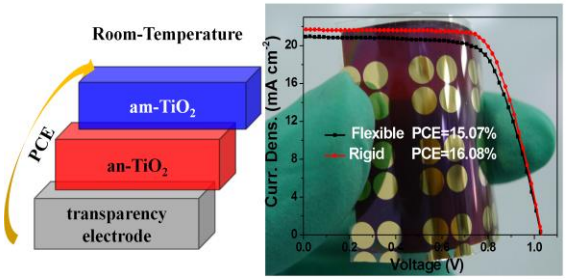

Broader Context

All high efficiency perovskite solar cells reported so far used high temperature (~500 ^{o}C) sintering to prepare metal oxides for electron transport layers. The high temperature treatment complicates the fabrication process, even worse, it excludes possibilities to make flexible cells using common polymeric substrates. It has been a challenge to fabricate an effective metal oxide electron transport layer for the flexible perovskite solar cell. In this work, we developed a process to fabricate very dense amorphous TiO_2 coating using DC magnetron sputtering at room temperature. It is found that the low temperature TiO_2 is amorphous in nature. It performs better in electron injection, hence reducing transfer resistance. The time-resolved photoluminescence spectroscopy shows that electrons transfer faster from the perovskite film to the amorphous-TiO_2 ETL than to the anatase-TiO_2, leading to strong steady state PL quenching in the FTO/ amorphous-TiO_2/perovskite films. The electrical impedance spectroscopy shows that the resistance is smaller for the amorphous-TiO_2 ETL, resulting in improved device performance.